

Cite this: *Dalton Trans.*, 2018, **47**, 12459

The bismuth oxyhalide family: thin film synthesis and periodic properties

Laura S. Gómez-Velázquez,^{a,b} Agileo Hernández-Gordillo,^b †^a Matthew J. Robinson,^c Valerie J. Leppert,^c Sandra E. Rodil,^b †^a and Monserrat Bizarro,^b *^a

Bismuth oxyhalides (BiOX, where X = F, Cl, Br, I) are interesting materials due to their layered structure, which can be useful for different applications. In this work, we present the synthesis of the complete BiOX family in the thin film form. The tetragonal phase Bi₂O₃ film deposited onto a glass substrate was transformed into BiOF, BiOCl or BiOBr by a simple immersion at ambient temperature in a halide (X = F, Cl, Br) containing solution. For these films, a residual phase from the oxide was present and for BiOF another phase (tentatively identified as Bi₇O₅F₁₁) was present too. For the BiOI film synthesis, an iodine and bismuth containing solution was sprayed onto the glass substrate heated at 275 °C and a pure phase was obtained. Microstructural and morphological characterization was performed by X-ray diffraction and scanning electron microscopy, while the chemical environment was studied by X-ray photoelectron spectroscopy. Optical and photocatalytic properties were also obtained. The physical and chemical characteristics of the BiOX films follow a correlation with the atomic radius of the halogen atom incorporated into the corresponding lattice. All the BiOX films showed a photocatalytic response for the photodiscoloration of indigo carmine dye under simulated sunlight irradiation in an alkaline medium. The photocatalytic reactions occurred via 2 proton–electron transfer from the oxide or oxyhalide to the adsorbed IC dye, favoring its reduction to the corresponding leuco IC form.

Received 28th June 2018,
Accepted 9th August 2018

DOI: 10.1039/c8dt02642d

rsc.li/dalton

1. Introduction

Bismuth is an element which is becoming the protagonist in novel binary, ternary and quaternary compounds. Beyond its use as a lead replacing element in alloys due to its low toxicity, recent investigations have shown its importance in the emerging low-dimensional materials for topological insulators,^{1–3} in perovskite structures for energy storage⁴ and photovoltaics,⁵ and for the design of other functional materials. Besides, bismuth is an abundant metal with a relatively low price, which is attractive for large scale applications.

Among the bismuth-based ternary compounds, bismuth oxyhalides (BiOX, X = F, Cl, Br, I) are a family which have recently attracted attention because of their layered growth that provide interesting potential applications in electronics,

and energy storage.^{6–8} This family presents a tetragonal matlockite structure consisting of [Bi₂O₂] layers sandwiched between double halide [X] layers, to form [X–Bi–O–Bi–X] layers held by van der Waals interactions through the halogen atom along the [001] direction.^{6,9–12} The arrangement of these layers provides a large space for the polarization of the atoms favoring the separation of photo-induced electron–hole pairs. Moreover, the high reactivity of specific facets, such as the {001} facet in BiOCl,¹³ has been demonstrated, making them attractive for photocatalysis and photoelectrochemical applications.¹⁴

There are recent studies reporting the photocatalytic properties of BiOX powders, especially for X = Cl, Br and I.^{15–17} There are also studies concerning the synthesis of bismuth oxyhalides as thin films where X = Cl, Br, I either by an aerosol assisted CVD method reported by Bhachu *et al.*⁹ or by a sol–gel method reported by Shen *et al.*¹⁸ In both cases, BiOX films showed photoactivity with BiOBr being the most active, but none of them included BiOF. BiOCl is the most studied bismuth oxyhalide, either in powder^{8,19,20} or thin film form.^{21–24} All reports show faceted laminar growth, which in some cases assembles to form flower-like structures. A diversity of methods have been used to individually obtain each halide of the family as thin films, such as MOCVD,²⁴ hydro-

^aInstituto de Investigaciones en Materiales, Universidad Nacional Autónoma de México, Circuito Exterior S/N, Ciudad Universitaria, Coyoacán, C.P. 04510, Ciudad de México, Mexico. E-mail: monserrat@iim.unam.mx

^bPosgrado en Ciencia e Ingeniería de Materiales, Universidad Nacional Autónoma de México, Mexico

^cDepartment of Materials Science and Engineering, University of California, Merced, CA 95343, USA

† Catedrático CONACYT.

lysis²³ or electrochemical methods²² for BiOCl, alcoholysis-coating methods for BiOBr,²⁵ or solvothermal synthesis for BiOI.²⁶ Unlike the synthesis of Bi₂O₃, in which the material's properties strongly depend on the growth technique, obtaining the oxyhalides seems relatively simple even at room temperature, especially with the use of wet methods. Previously, the transformation of a β -Bi₂O₃ film into pure BiOCl due to its contact with a HCl solution was reported.²⁷ This was a favorable reaction ($\Delta E = -569.8 \text{ kJ mol}^{-1}$), considering the difference between the Gibbs energy of the products and the reactants. Due to its reactivity, the Cl⁻ ion penetrated the Bi₂O₃ lattice and substituted the O atom, changing the compound and its structure.

In this work, we report relatively simple methods to obtain the complete BiOX film family. The BiOF, BiOCl, and BiOBr thin films were chemically transformed from original spray deposited tetragonal Bi₂O₃ by an immersion procedure of the films in the corresponding halogenated solution. The degree of transformation strongly depended on the nature of the solutions. For the BiOI films, a direct atomization method was used. After a complete characterization of the different films, we observed periodic behaviors of the structural, morphological and optical properties with respect to the atomic radius of each halogen. Their photocatalytic activity was tested by the photodiscoloration of an indigo carmine dye solution *via* the formation of leuco indigo carmine under simulated sunlight.

2. Experimental details

2.1 Synthesis of BiOF, BiOCl and BiOBr films

For the first three ternary compounds of the family, we started from a Bi₂O₃ film that was obtained by the pneumatic spray pyrolysis method previously reported.²⁷ In summary, we used bismuth(III) acetate (Bi(CH₃CO₂)₃, 98% from Sigma Aldrich) dissolved in acetic acid (25% of the total solution's volume) at 45 °C under constant stirring for one hour and then added 75% deionized water to obtain a completely transparent homogeneous solution. This solution was sprayed onto clean glass substrates at 450 °C with solution and gas flow rates of 7.7 mL min⁻¹ and 9.6 L min⁻¹, respectively.

Each of the resultant Bi₂O₃ films were immersed in a chemical bath of the corresponding solution (KBr, HCl and HF) at ambient temperature as indicated in Table 1. As the prepared solutions were corrosive, the films suffered surface

etching, and transformation of the oxide into the oxyhalide was achieved, as shown in the Results section.

2.2 Synthesis of BiOI films

The chemical bath method used for the previous samples was not adequate to obtain good quality BiOI films using either ammonium iodide or potassium iodide solutions for the bath. The chemical reactions with the NH₄I solution produced cracking of the films and diminished its adhesion to the substrate. The films obtained in this way presented a mixture of phases (Bi₂O₃, BiOI and non-stoichiometric bismuth oxyiodide) that could not be transformed into pure BiOI. In order to avoid these drawbacks, we decided to deposit this material by spraying a precursor solution containing 0.02 M bismuth nitrate (Bi(NO₃)₃ · 5H₂O, >98% Sigma Aldrich) and 0.04 M NH₄I (% Sigma-Aldrich) dissolved in ethylene glycol (C₂H₆O₂, 99%, Sigma Aldrich).²⁸ Precursor solutions were manually sprayed onto 275 °C substrates.

2.3 Characterization

X-ray diffraction (XRD) patterns were acquired with a Rigaku-Ultima IV system (Cu K α = 1.5406 Å, 40 kV, 44 mA) equipped with a thin film stage. For the identification of the diffraction peaks and the calculation of the lattice parameters, the software PDXL2® was used. Scanning electron microscopy (SEM) was performed on the films to analyze the surface morphology with a JEOL 7600F microscope. The thickness of the films was measured with a Veeco Dektak 150 profilometer. Optical properties were studied by diffuse reflectance UV-Vis spectroscopy (DRS) on a Shimadzu 2600 spectrophotometer using BaSO₄ as a reference. The spectra were converted from reflectance to absorbance by the Kubelka–Munk method to calculate the band gap energy (E_g) of the films. X-ray photoelectron spectroscopy (XPS) was performed on the films with an ultra-high vacuum system scanning XPS microprobe PHI 5000 Versa Probe II of Physical Electronics. A monochromated Al K α ($h\nu = 1486.6 \text{ eV}$) X-ray source was used at 25 W with 100 μm beam diameter. The surface of each sample was etched for 3 min with 1 kVAr⁺ at 55.56 nA mm⁻². The XPS spectra were acquired at 45° from the surface in a constant pass energy mode (CAE) at $E_0 = 117.40$ and 11.75 eV for survey and high-resolution spectra, respectively.

2.4 Photocatalytic tests

The photocatalytic response of the different BiOX materials was evaluated by the photodiscoloration reaction of an aqueous solution of the organic dye indigo carmine (IC) at a concentration of 5 mg L⁻¹ and pH ~ 11–12. The pH was adjusted by adding NaOH to reduce the adsorption of IC molecules on the photocatalyst surfaces. Prior to illumination, the samples were kept for 30 minutes in the dark with constant stirring; this time was enough to reach the adsorption–desorption equilibrium. The illumination source was a solar simulator Oriel 96000 (150 W, irradiance of 360 Wm⁻²). The photodiscoloration process was monitored by following the absorbance spectrum of the IC dye as a function of the

Table 1 Conditions of the chemical baths

Film material	Chemical bath solution	Immersion time
BiOF	HF (0.03 M) in deionized water	15 min
BiOCl	HCl (0.15 M) in deionized water	60 min
BiOBr	KBr (0.1 M) and acetic acid (0.03 M) in deionized water	90 min

irradiation time. The discoloration percentage was calculated as:

$$\text{Discoloration \%} = \left(1 - \frac{A(t)}{A_0}\right) \times 100$$

where $A(t)$ and A_0 are the absorbance at an irradiation time t and the initial absorbance, respectively, of the typical band of the IC dye solution ($\lambda = 610$ nm at pH ~ 11 –12).

3. Results

3.1 Crystalline structure

Fig. 1 shows the diffraction patterns of the different oxyhalides, including the original Bi_2O_3 film that corresponds to the tetragonal crystal structure –named β phase– according to the ICDD PDF no. 01-078-1793. It is worth mentioning that Bi_2O_3 presents 6 polymorphs, but under the spray deposition conditions used, only the tetragonal β - Bi_2O_3 was obtained. When the β - Bi_2O_3 film was immersed in the HF aqueous solution, Bi_2O_3 was transformed into the oxyfluoride, shown in Fig. 1 with peaks indexed from BiOF (PDF 01-073-1595), along with another phase, tentatively identified as $\text{Bi}_7\text{O}_5\text{F}_{11}$ (PDF 050-0003) and some remaining β - Bi_2O_3 . For the film immersed in HCl, the peaks of BiOCl were detected and indexed to the ICDD file no. 01-082-0485; the peak at 27.9° corresponds to residual β - Bi_2O_3 (*). For the bromide film, the pattern corresponds to file 01-073-2061 of BiOBr , but there is also the presence of the original β - Bi_2O_3 phase (*). The sprayed iodide film resulted in the pure BiOI phase indexed to the file no. 01-073-2062. In this last case, the residual β - Bi_2O_3 phase was not detected as the BiOI film was formed directly. X-ray photoelectron spectroscopy (XPS) chemical shift data, dis-

cussed below, also confirm the formation of the bismuth oxyhalides.

Bi_2O_3 belongs to the space group $P\bar{4}21c$, and the complete oxyhalide family has a $P4/nmm$ space group. It is interesting to note that the tetragonal structure remains, but the lattice parameters change, with the increasing atomic radius of the halogen, following the periodic table's trend, as shown schematically in Fig. 2. The obtained lattice parameters coincide with the calculated values reported by A. Ganose *et al.*¹² and Huang *et al.*^{29,30} for BiOX and by Li *et al.*³¹ for β - Bi_2O_3 , showing very small variations as shown in Table 2. The crystallite size was calculated using Scherrer's formula and the values are given in Table 2. In this case, the average crystal size is smaller for the oxyhalide where the halogen's atomic radius is larger.

3.2 XPS analysis

Chemical analysis of the films was performed using the XPS technique. Fig. 3a shows the high-resolution spectra of the halogen peaks corresponding to F 1s, Cl 2p, Br 3d and I 4d orbitals with their corresponding deconvolutions indicating the spin-orbit splitting from a single oxidation state. The binding energy of the halogens is in agreement with the reported values.³² In addition, Fig. 3b shows the spectra of the Bi 4f orbitals in β - Bi_2O_3 and the BiOX films. The spectra show Bi in two oxidation states, Bi^{3+} and Bi^0 ; two minor peaks centered at 159.79 and 157.90 eV are related to the Bi^0 metallic state (chemical shift reported between Bi and Bi^{3+} is 2.0 eV (ref. 33)). This is probably a consequence of a slight reduction of Bi^{3+} occurring during the Ar cleaning.³⁴ The larger spin-orbit peaks that showed a shift to larger binding energies, as

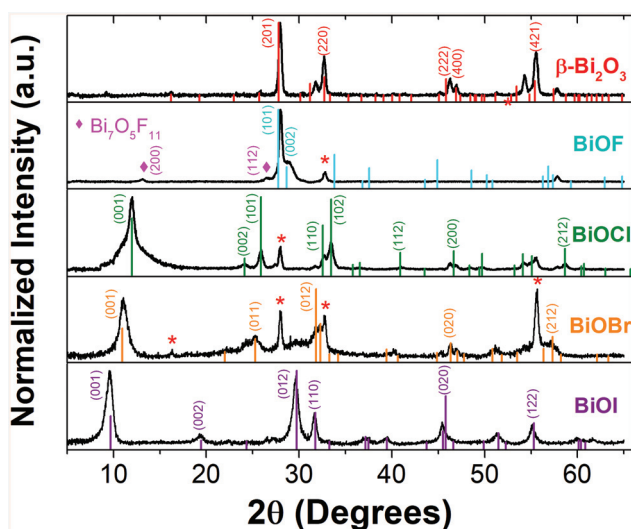


Fig. 1 XRD patterns of the Bi_2O_3 film and the oxyhalide family. The vertical lines are the positions of the corresponding BiOX ICDD file, and the peaks marked with * correspond to β - Bi_2O_3 . For the BiOF film, the peaks marked with ♦ correspond to the $\text{Bi}_7\text{O}_5\text{F}_{11}$ phase.

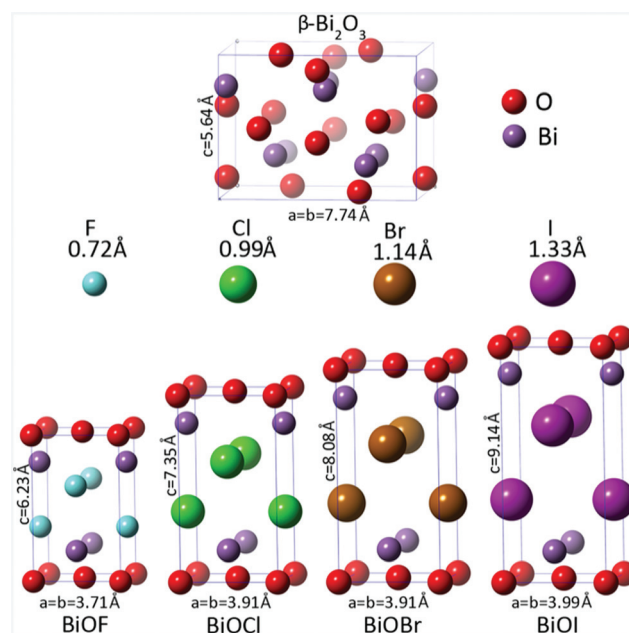


Fig. 2 Schematic representation of the unit cells of Bi_2O_3 and BiOX ($X = \text{F}, \text{Cl}, \text{Br}, \text{I}$).

Table 2 Lattice parameters and crystallite size of BiOX films

Compound	Halogen's atomic radius (Å)	Lattice parameters (Å)	Deviation from the values calculated by DFT	Crystallite size (nm)
β -Bi ₂ O ₃	—	$a = b = 7.74, c = 5.64$	$a: -0.25\%; c: 2.48\%^{31}$	22.2
BiOF	0.72	$a = b = 3.71, c = 6.23$	$a: -0.27\%; c: 0.48\%^{12}$	22.5
BiOCl	0.99	$a = b = 3.91, c = 7.35$	$a: +1.02\%; c: -0.95\%^{12}$	9.0
BiOBr	1.14	$a = b = 3.91, c = 8.08$	$a: +0.25\%; c: -0.74\%^{12}$	9.7
BiOI	1.33	$a = b = 3.99, c = 9.14$	$a: +0.25\%; c: -0.11\%^{12}$	9.5

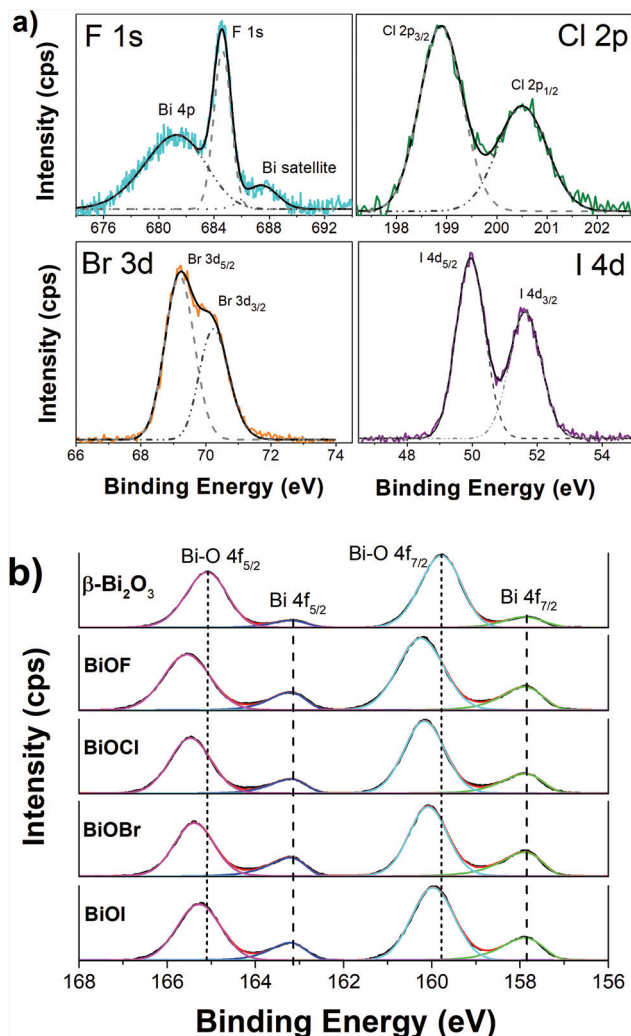


Fig. 3 (a) High resolution spectra of the halogen orbitals (F 1s, Cl 2p, Br 3d and I 4d). (b) Binding energy (eV) of the Bi 4f_{7/2} orbital in β -Bi₂O₃ and BiOX films.

the electronegativity of the halogen atom increases, correspond to the Bi–O for the β -Bi₂O₃ films and the Bi–O–X bonds. Fluorine is the most electronegative of the halogens (and of the elements) and its binding energy in the Bi 4f_{7/2} orbital is 160.25 eV, which is the largest value among all in the family. Conversely, BiOI has the smallest value, 159.98 eV, as I is the least electronegative element of the halide family. In all oxyhalides, the signals of the Bi⁰ metallic state were also observed in greater proportion than of the β -Bi₂O₃ film. In Table 3 are the binding energy values and the binding energy shift (Δ BE) from the Bi 4f_{7/2} orbital, which decreases while the atomic radius of the halogen increases (following the periodic table's trend).

3.3 Morphology

Fig. 4 shows the SEM images of the β -Bi₂O₃ film and the oxyhalides. The original sprayed pyrolyzed β -Bi₂O₃ film has a compact surface with irregular agglomerated grains on the top (Fig. 4a). After the chemical bath treatment, the BiOF film presents a more granulated surface in which these grains are better defined (Fig. 4b). The HCl chemical bath treatment of the Bi₂O₃ film provoked a faceted structure, evidenced by thin plates with rounded ends (Fig. 4c). This trend continues for the chemical bath with KBr, giving a flake-like morphology of the BiOBr film (Fig. 4d). In this film, the nanoplates or nanoflakes are better defined, thinner and denser than in the BiOCl film. However, some irregular agglomerated grains corresponding to the β -Bi₂O₃ phase were also observed. Finally, for the sprayed BiOI film, very large thin plates appear randomly oriented, giving a highly porous and rough surface (Fig. 4e and f). Comparing the complete BiOX family, it is an evident evolution of the morphology towards a lamellar structure as the atomic radius of the halogen increases. This lamellar morphology is typically observed for BiOX films grown by different techniques, although some of them allow the formation of defined platelets easier.⁹

3.4 Optical properties

As a first approximation, we used DRS to evaluate the optical properties of the films, since they present an opaque aspect

Table 3 Binding energies, electronegativities and bandgap energies of the BiOX films

Material	Bi 4f _{7/2} (eV)	Δ BE (eV)	Electronegativity of the X atom	E_g (eV) measured	E_g (eV) reported
Bi ₂ O ₃	159.79	0	—	2.6	2.4–2.8 ^{35,36}
BiOF	160.25	0.46	3.98	3.7	3.64 ³⁷
BiOCl	160.17	0.38	3.16	3.6	3.2–3.5 ^{9,15–17}
BiOBr	160.08	0.29	2.96	2.5	2.6–2.8 ^{9,15–17,25}
BiOI	159.98	0.19	2.66	2.0	1.7–1.9 ^{9,15–17,38,39}

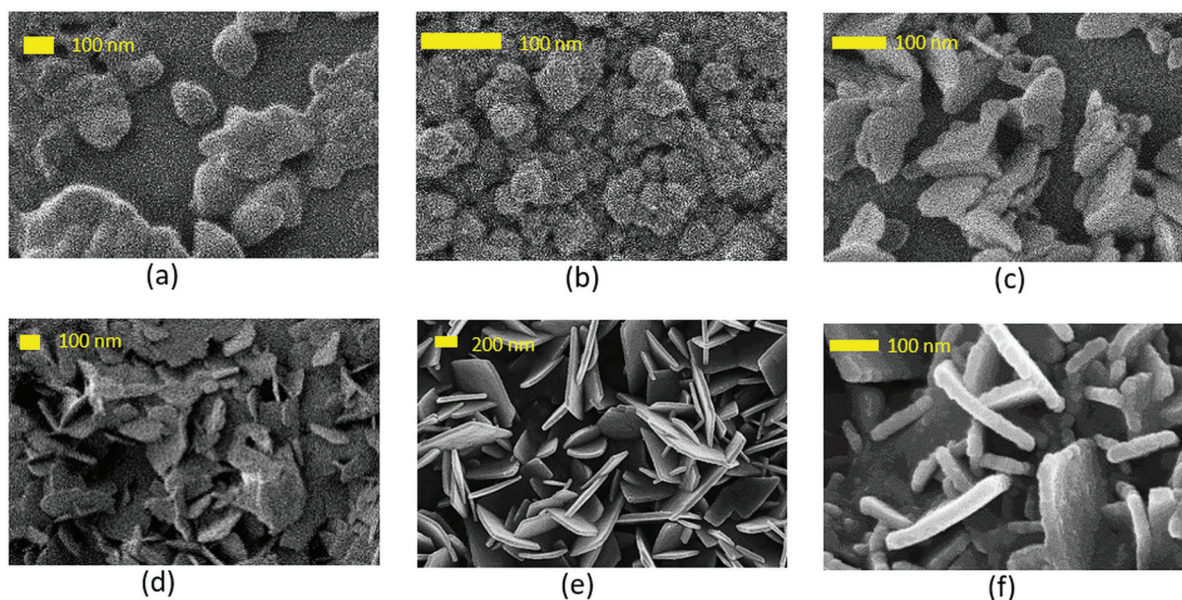


Fig. 4 SEM images of (a) Bi_2O_3 , (b) BiOF , (c) BiOCl , (d) BiOBr , (e) and (f) BiOI films.

and their transmittance was very low (less than 10% for wavelengths shorter than 800 nm). The energy band gap (E_g) was estimated by calculating the absorption coefficient through the Kubelka–Munk (K–M) function $F(R_\infty)$:

$$\frac{K}{S} = \frac{(1 - R_\infty)^2}{2R_\infty} \equiv F(R_\infty) \cong \alpha$$

where K and S are the Kubelka–Munk coefficients and $R_\infty = R_{\text{sample}}/R_{\text{reference}}$ is the reflectance. E_g values were calculated inferring indirect transitions¹¹ considering that the materials are thin films and have a lot of surface defects; hence plots of $(F(R_\infty) \cdot h\nu)^{1/2}$ vs. E were obtained and the E_g value was calculated by the extrapolation of the linear part to the horizontal axis, as shown in Fig. 5. The obtained E_g values appear in Table 3; again, this characteristic decrease following the periodic table's trend of the halogen group. Table 3 also lists the E_g values reported in previous studies, but most of them are for the materials in powder form.

3.5 Photocatalytic properties

The photocatalytic activity of Bi_2O_3 and the BiOX family films was tested by following the photodiscoloration of IC dye at pH 12 under simulated sunlight (Fig. 6a and b). Under these conditions, the photolysis reached less than 12% discoloration. Fig. 6a shows the absorbance spectrum of IC dye solution during the adsorption process in the dark (dashed line) and its evolution as the time progresses until 180 min of reaction in contact with the original Bi_2O_3 film under simulated sunlight. The peak located at 610 nm suffers a large decrease with time, disappearing almost completely. The decrease of this absorbance band is clearly observed and it is related to the discoloration of the IC dye solution. The analysis of the spectral changes in the UV range (240–270 nm) indicates that the

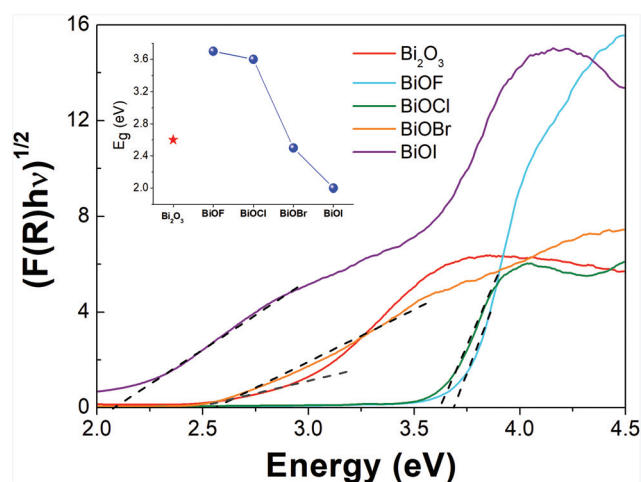


Fig. 5 DRS of $\beta\text{-Bi}_2\text{O}_3$ and BiOX films, where the absorption edges are marked with dotted lines. The inset shows the change of E_g for the BiOX family films.

photodiscoloration pathway that took place during the photocatalytic reaction was the reduction of the IC into the leuco IC form. This reduction occurred *via* a 2 proton–electron transfer reaction in an alkaline medium with the subsequent hydrogenation.^{40,41} Furthermore, the formation of leuco IC is confirmed by two isosbestic points (at 363 and 444 nm, clearly seen in Fig. 6a) according to the previously reported work.⁴²

A similar absorbance time-evolution was observed for the BiOX films, so Fig. 6b shows the absorbance spectrum of the IC dye solution after 180 min of reaction in contact with each one of the formed oxyhalides (BiOX films) under simulated sunlight. In all cases, the band at 610 nm suffered a large decrease, especially for the BiOCl film, for which this peak

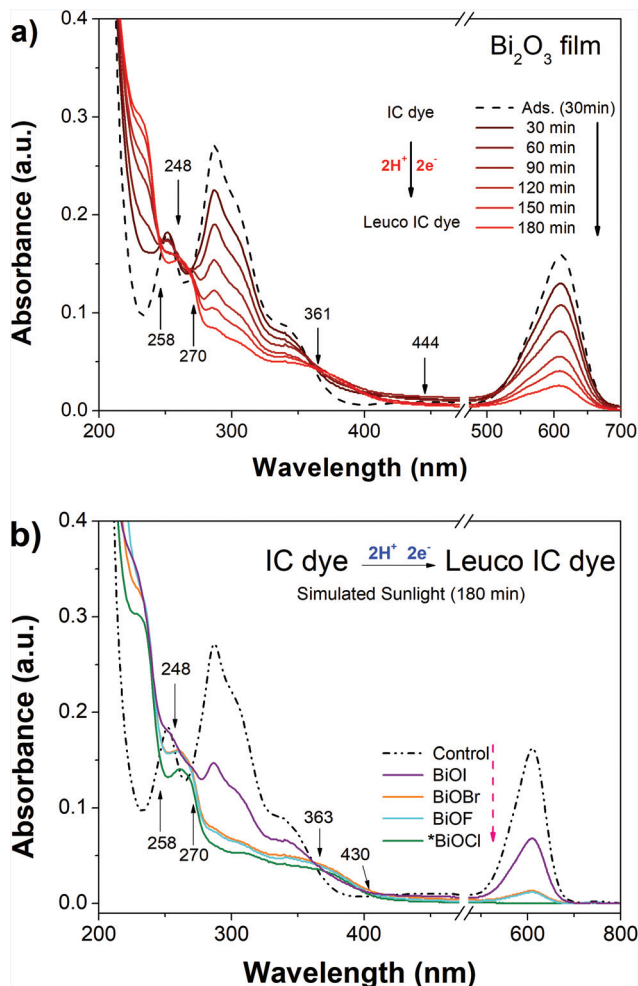


Fig. 6 Absorbance spectra of IC dye during simulated sunlight irradiation: (a) using the $\beta\text{-Bi}_2\text{O}_3$ film and (b) after 180 min of irradiation in the presence of BiOX films (except for BiOCl where the irradiation time is 90 min).

completely disappeared. The presence of five isosbestic points (258, 248, 270, 363 and 430 nm, Fig. 6b) indicates that the photodiscoloration process of IC dye was due to the transformation to its corresponding leuco IC form.

The percentage of discoloration achieved after 180 min for the Bi_2O_3 and all the BiOX family films is presented in Fig. 7. The BiOCl film achieved $\sim 97\%$ discoloration in only 90 min of sunlight irradiation, while the BiOI film exhibited the lowest response achieving $\sim 58\%$ discoloration after 180 min. BiOF, BiOBr and Bi_2O_3 presented also very good response with percentages between 84 and 92% in the same 180 min. It can be noted that the adsorption of the IC dye onto the films was negligible in all cases, suggesting that the discoloration process was achieved *via* the reduction reaction.

3.6 Calculated energy diagram

Based on the electronegativity of each atom, the energy diagram of Bi_2O_3 and the BiOX family was calculated. Assuming a Nernstian behavior in aqueous solution for all the

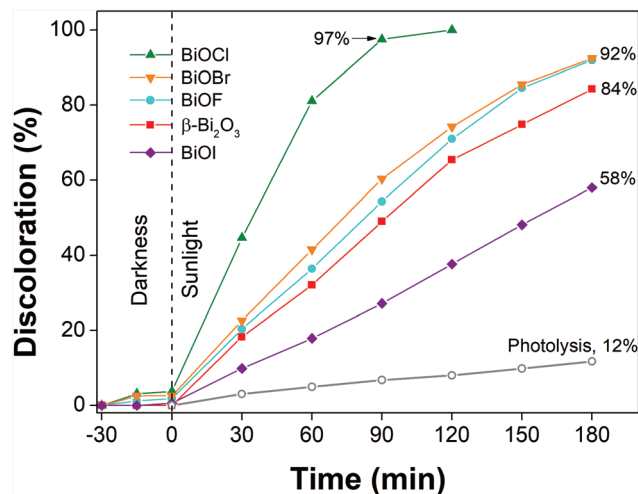


Fig. 7 Discoloration efficiency of IC dye at pH 12 by using $\beta\text{-Bi}_2\text{O}_3$ and the different BiOX films under simulated sunlight. Photolysis of the IC dye solution is also included.

materials, the band edge positions were plotted as a function of the pH solution *vs.* NHE (Fig. 8). Under the standard conditions (at pH = 0), the values of the conduction band of Bi_2O_3 and BiOCl (Fig. 8a) are more negative (-0.03 and -0.16 V) than those of BiOF, BiOBr and BiOI (Fig. 8b) which are positive (>0.26 V). However, according to the calculations, under the conditions of the photocatalytic reaction test (pH ~ 12), the calculated value of the band-edge position for BiOF, BiOBr and BiOI may be displaced to more negative energies, reaching values of -0.44 ± 0.01 V, whereas for Bi_2O_3 and BiOCl it is changed to -0.7 and -0.87 V, which results in a higher reducing power. On the other hand, the redox potential of the couple IC/leuco IC at the same pH ~ 12 is -0.144 V *vs.* NHE (-0.53 V *vs.* Ag/AgCl)^{40,41} and for the couple $\text{O}_2/\text{O}_2^{*2-}$ it is -0.133 V *vs.* NHE.⁴³

4. Discussion

We have shown that it is possible to gradually transform the $\beta\text{-Bi}_2\text{O}_3$ structure to BiOX (X = F, Cl, Br) by immersion in a halogen containing solution at ambient temperature. Due to the electronegativity and the electronic configuration of the X halogen atoms (which have a p^5 orbital avid for electrons), these X atoms penetrate into the tetragonal Bi_2O_3 lattice by substituting the central oxygen layer. The chemical reactions for the transformation of bismuth oxide to the corresponding oxyhalide are expressed below:



for BiOF, BiOCl and BiOBr, respectively. The chemical nature of the immersion bath is an important factor for the duration

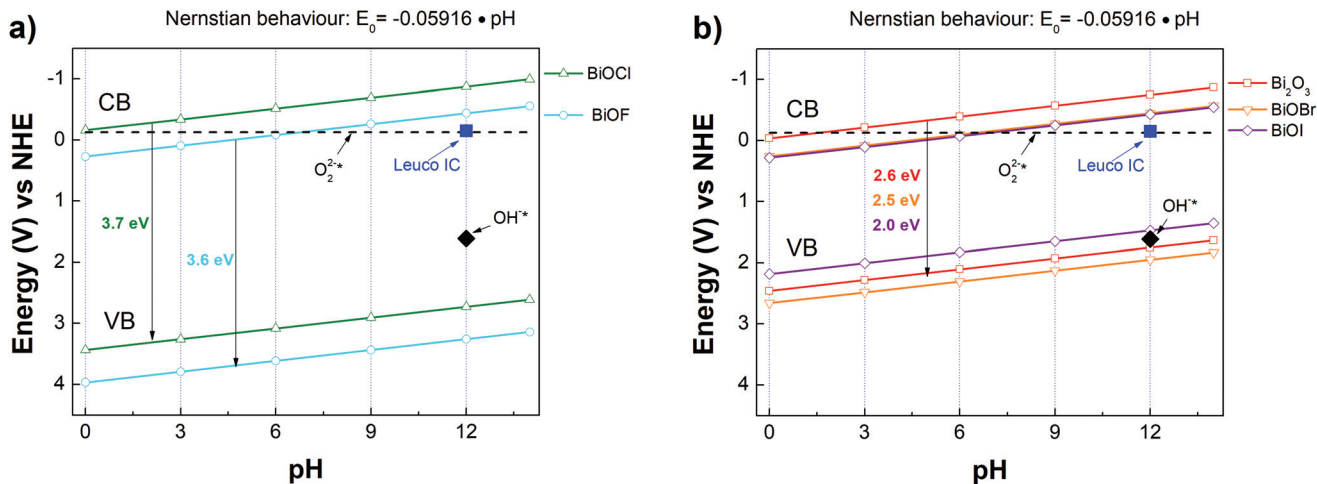


Fig. 8 (a and b) Energy diagram of the band-edge positions for the Bi_2O_3 and BiOX family as a function of the solution pH. The redox potential of the couple IC/leuco IC and $\text{O}_2/\text{O}_2^{\cdot 2-}$ is also included.

of the transformation process. When using HF solution, the immersion time was shorter than that for the other solutions even though the molar concentration of the solution was lower. Due to the fast transformation of Bi_2O_3 into BiOF , it was difficult to precisely control the formation of a pure BiOF phase. For 15 min of immersion in HF solution, the XRD pattern shows a majority of BiOF , but also a $\text{Bi}_7\text{O}_5\text{F}_{11}$ phase along with the original $\beta\text{-Bi}_2\text{O}_3$. For larger immersion times in HF, the etching of the film was strong enough to detach the film from the substrate, while for shorter immersion times the transformation was incipient and the presence of Bi_2O_3 dominated. In the case of the BiOCl film, the transformation took a longer time (60 min of immersion), for which the film still had the presence of some residual Bi_2O_3 , but a balance had to be made to avoid the detachment of the film from the substrate. When using the KBr in acetic acid solution, the transformation of Bi_2O_3 into BiOBr was even slower (90 min of immersion), and due to that some remaining peaks of $\beta\text{-Bi}_2\text{O}_3$ were also observed in the XRD pattern.

The BiOI sprayed film presented a pure phase that could not be achieved with the several chemical baths' conditions tested; hence, the spraying method is good to obtain this material, in accordance with the published studies^{9,28} that also report good adhesion of the film to the substrate. The spray pyrolysis technique may have some advantages for growing BiOX films, as it is a one-step process and does not present the etching/detachment of the film, as it occurs during the chemical bath immersion of the Bi_2O_3 film. One has just to be aware of the precursor solutions to be sprayed in order to obtain a good quality film.

Here we demonstrate the easiness to transform the bismuth oxide into the oxyhalide, but the conditions of the chemical baths can still be optimized in order to obtain pure phases. Even though the transformation for some samples was not complete, the presence of the oxyhalide was sufficient to show important changes in all their physicochemical properties.

Most of these properties follow a trend while going down along the halogen's group in the periodic table. As the halogen's atomic radius increases, the lattice parameters also increase; the morphology evolves from irregular grains to sharper and more defined laminar structures. The electronegativity decreases as $\text{F} > \text{Cl} > \text{Br} > \text{I}$ and so does the binding energy in the $\text{Bi } 4f_{7/2}$ orbital shifts and the energy bandgaps while going down in the group from 3.7 to 2.0 eV. BiOF and BiOCl absorb only UV-C light, whereas BiOBr and BiOI can absorb light from the visible region. Finally, Bi_2O_3 and all the oxyhalides presented photocatalytic activity response for the photodiscoloration of IC dye in an alkaline medium ($\text{pH} \sim 12$) under simulated sunlight. The photocatalytic reaction occurred *via* 2 proton–electron transfer reactions from the oxide or oxyhalide surface material to the adsorbed IC dye, reducing/hydrogenating to its corresponding leuco IC dye. The electron transfer process observed for all materials can be explained because in the alkaline medium ($\text{pH} \sim 12$), they have enough negative potential (-0.4 to -0.9 V *vs.* NHE) to reduce the IC dye (-0.144 V *vs.* NHE). Despite the fact that BiOF and BiOCl can only absorb UV-C light, they exhibited a high rate of electron transfer, whereas for BiOI which absorbs visible light, the low rate of electron transfer could be affected by the lamellar morphology, which leads to the change in the exposed surface area.

5. Conclusions

The thin film bismuth oxyhalide family BiOX was obtained by a chemical bath treatment of a sprayed pyrolyzed Bi_2O_3 film in the case of $\text{X} = \text{F}, \text{Cl}$ and Br , whereas the BiOI film was produced by a direct spraying of an iodine and bismuth containing solution. Immersion of the $\beta\text{-Bi}_2\text{O}_3$ film in the corresponding halogenated solution causes a gradual transformation of the oxide into the oxyhalide, but the degree of transform-

ation strongly depends on the nature of the bath solution. The physical and chemical characteristics of these compounds follow the same trend as the halogen atoms in the periodic table: lattice parameters and lamellar morphology increase with the halogen's increasing atomic radius; binding energy shifts and the optical band gap decrease as the halogen's atomic radius increases. All the oxyhalides have the conduction band minimum at enough negative potential leading to a good photocatalytic response under simulated sunlight for the reduction of indigo carmine dye into leuco IC in the alkaline medium. BiOCl showed the highest photocatalytic performance even though it only absorbs UV-C light, this is due to its higher reductive power compared to the other oxyhalides.

Conflicts of interest

There are no conflicts of interest to declare.

Acknowledgements

The authors are grateful to Adriana Tejada, Omar Novelo, Josué Ibarra, Lázaro Huerta, Juan Manuel García-León, Carlos Ramos and Estrella Ramos for technical support during the characterization of the films. This work was supported by DGPA-PAPIIT under projects IN106015 and IN108618. Financial support from CONACYT project 251279 is also acknowledged.

References

- 1 R. R. Q. Freitas, *et al.*, Spin-orbit-induced gap modification in buckled honeycomb XBi and XBi₃ (X = B, Al, Ga, and In) sheets, *J. Phys.: Condens. Matter*, 2015, **27**(48), 485306.
- 2 F.-C. Chuang, *et al.*, Prediction of Large-Gap Two-Dimensional Topological Insulators Consisting of Bilayers of Group III Elements with Bi, *Nano Lett.*, 2014, **14**(5), 2505–2508.
- 3 R. R. Q. Freitas, *et al.*, Tuning band inversion symmetry of buckled III-Bi sheets by halogenation, *Nanotechnology*, 2016, **27**(5), 055704.
- 4 F. Li, *et al.*, Exploring novel bismuth-based materials for energy storage applications, *J. Mater. Chem. C*, 2018, **6**, 7976–7981.
- 5 N. C. B. Miller and M. Bernechea, Research Update: Bismuth based materials for photovoltaics, *APL Mater.*, 2018, **6**(8), 084503.
- 6 J. Li, Y. Yu and L. Zhang, Bismuth oxyhalide nano-materials: layered structures meet photocatalysis, *Nanoscale*, 2014, **6**(15), 8473–8488.
- 7 M. Guan, *et al.*, Vacancy associates promoting solar-driven photocatalytic activity of ultrathin bismuth oxychloride nanosheets, *J. Am. Chem. Soc.*, 2013, **135**(28), 10411–10417.
- 8 K.-L. Zhang, *et al.*, Study of the electronic structure and photocatalytic activity of the BiOCl photocatalyst, *Appl. Catal., B*, 2006, **68**(3), 125–129.
- 9 D. S. Bhachu, *et al.*, Bismuth oxyhalides: synthesis, structure and photoelectrochemical activity, *Chem. Sci.*, 2016, **7**(8), 4832–4841.
- 10 F. Bannister and M. Hey, The crystal structure of the bismuth oxyhalides, *Mineral. Mag.*, 1935, **24**, 49–58.
- 11 M. A. Gondal, C. Xiaofeng and M. A. Dastageer, *Novel Bismuth-Oxyhalide-Based Materials and their Applications*, Springer India, 2017.
- 12 A. M. Ganose, *et al.*, Interplay of Orbital and Relativistic Effects in Bismuth Oxyhalides: BiOF, BiOCl, BiOBr, and BiOI, *Chem. Mater.*, 2016, **28**(7), 1980–1984.
- 13 J. Jiang, *et al.*, Synthesis and Facet-Dependent Photoreactivity of BiOCl Single-Crystalline Nanosheets, *J. Am. Chem. Soc.*, 2012, **134**(10), 4473–4476.
- 14 X. Xiao, *et al.*, Oxygen-rich bismuth oxyhalides: generalized one-pot synthesis, band structures and visible-light photocatalytic properties, *J. Mater. Chem.*, 2012, **22**(43), 22840–22843.
- 15 A. Huizhong, *et al.*, Photocatalytic properties of BiOX (X = Cl, Br, and I), *Rare Met.*, 2008, **27**(3), 243–250.
- 16 X. Chang, *et al.*, BiOX (X = Cl, Br, I) photocatalysts prepared using NaBiO₃ as the Bi source: characterization and catalytic performance, *Catal. Commun.*, 2010, **11**(5), 460–464.
- 17 X. Zhang, *et al.*, Generalized one-pot synthesis, characterization, and photocatalytic activity of hierarchical BiOX (X = Cl, Br, I) nanoplate microspheres, *J. Phys. Chem. C*, 2008, **112**(3), 747–753.
- 18 F. Shen, *et al.*, Preparation and characterization of SiO₂/BiOX (X = Cl, Br, I) films with high visible-light activity, *RSC Adv.*, 2015, **5**(7), 4918–4925.
- 19 Y. Lei, *et al.*, Synthesis, characterization and assembly of BiOCl nanostructure and their photocatalytic properties, *CrystEngComm*, 2009, **11**(9), 1857–1862.
- 20 L.-P. Zhu, *et al.*, Self-assembled 3D BiOCl architectures: tunable synthesis and characterization, *CrystEngComm*, 2010, **12**(11), 3791–3796.
- 21 C. Sihai, *et al.*, A novel BiOCl film with flowerlike hierarchical structures and its optical properties, *Nanotechnology*, 2009, **20**(27), 275702.
- 22 X. Zhang, *et al.*, A novel BiOCl thin film prepared by electrochemical method and its application in photocatalysis, *Appl. Catal., B*, 2013, **132–133**, 332–341.
- 23 S. Wu, C. Wang and Y. Cui, Controllable growth of BiOCl film with high percentage of exposed {001} facets, *Appl. Surf. Sci.*, 2014, **289**, 266–273.
- 24 P. Jagdale, *et al.*, Nano sized bismuth oxy chloride by metal organic chemical vapour deposition, *Appl. Surf. Sci.*, 2014, **303**, 250–254.
- 25 R. Li, *et al.*, Preparation of BiOBr thin films with micro-nano-structure and their photocatalytic applications, *Thin Solid Films*, 2014, **562**, 506–512.

- 26 S. Cui, G. Shan and L. Zhu, Solvothermal synthesis of I-deficient BiOI thin film with distinct photocatalytic activity and durability under simulated sunlight, *Appl. Catal., B*, 2017, **219**, 249–258.
- 27 K. Barrera-Mota, *et al.*, Spray deposited beta-Bi₂O₃ nanostructured films with visible photocatalytic activity for solar water treatment, *Photochem. Photobiol. Sci.*, 2015, **14**(6), 1110–1119.
- 28 N. T. Hahn, *et al.*, Spray pyrolysis deposition and photoelectrochemical properties of n-type BiOI nanoplatelet thin films, *ACS Nano*, 2012, **6**(9), 7712–7722.
- 29 W. L. Huang and Q. Zhu, DFT calculations on the electronic structures of BiOX (X = F, Cl, Br, I) photocatalysts with and without semicore Bi 5d states, *J. Comput. Chem.*, 2009, **30**(2), 183–190.
- 30 W. L. Huang, Electronic structures and optical properties of BiOX (X = F, Cl, Br, I) via DFT calculations, *J. Comput. Chem.*, 2009, **30**(12), 1882–1891.
- 31 Q.-Y. Li and Z.-Y. Zhao, Interfacial properties of α/β -Bi₂O₃ homo-junction from first-principles calculations, *Phys. Lett. A*, 2015, **379**(42), 2766–2771.
- 32 A. V. Naumkin, A. Kraut-Vass, S. W. Gaarenstroom and C. J. Powell, <https://srdata.nist.gov/xps/>, 2012 September 15, 2012. [cited 2017 April, 2017]; available from: <https://srdata.nist.gov/xps/>.
- 33 G.-H. Hwang, *et al.*, An electrochemical sensor based on the reduction of screen-printed bismuth oxide for the determination of trace lead and cadmium, *Sens. Actuators, B*, 2008, **135**(1), 309–316.
- 34 K. Uchida and A. Ayame, Dynamic XPS measurements on bismuth molybdate surfaces, *Surf. Sci.*, 1996, **357–358**, 170–175.
- 35 Y. Yan, *et al.*, Template-free fabrication of α - and β -Bi₂O₃ hollow spheres and their visible light photocatalytic activity for water purification, *J. Alloys Compd.*, 2014, **605**(Supplement C), 102–108.
- 36 X. Xiao, *et al.*, Facile large-scale synthesis of β -Bi₂O₃ nanospheres as a highly efficient photocatalyst for the degradation of acetaminophen under visible light irradiation, *Appl. Catal., B*, 2013, **140–141**(Supplement C), 433–443.
- 37 W. Su, *et al.*, Synthesis and catalytic performances of a novel photocatalyst BiOF, *Scr. Mater.*, 2010, **62**(6), 345–348.
- 38 L. Yosefi and M. Haghghi, Fabrication of nanostructured flowerlike p-BiOI/p-NiO heterostructure and its efficient photocatalytic performance in water treatment under visible-light irradiation, *Appl. Catal., B*, 2018, **220**(Supplement C), 367–378.
- 39 J. Xu, *et al.*, Polypyrrole decorated BiOI nanosheets: Efficient photocatalytic activity for treating diverse contaminants and the critical role of bifunctional polypyrrole, *J. Colloid Interface Sci.*, 2017, **505**(Supplement C), 719–727.
- 40 N. Sridivya, *et al.*, Two-step reduction of indigo carmine by dithionite: a stopped-flow study, *J. Chem. Soc., Faraday Trans.*, 1994, **90**(17), 2525–2530.
- 41 J. Carretero-Gonzalez, E. Castillo-Martinez and M. Armand, Highly water-soluble three-redox state organic dyes as bifunctional analytes, *Energy Environ. Sci.*, 2016, **9**(11), 3521–3530.
- 42 A. Hernández-Gordillo, *et al.*, Photodegradation of Indigo Carmine dye by CdS nanostructures under blue-light irradiation emitted by LEDs, *Catal. Today*, 2016, **266**, 27–35.
- 43 J. C. Medina, *et al.*, Synergistic effect of supported ZnO/Bi₂O₃ heterojunctions for photocatalysis under visible light, *Dyes Pigm.*, 2018, **153**, 106–116.